

Self-Assembly Formed by Spherical Patchy Particles with Long-Range Attraction

メタデータ	言語: eng 出版者: 公開日: 2019-09-06 キーワード (Ja): キーワード (En): 作成者: メールアドレス: 所属:
URL	https://doi.org/10.24517/00055375

This work is licensed under a Creative Commons Attribution-NonCommercial-ShareAlike 3.0 International License.



Self-Assembly Formed by Spherical Patchy Particles with Long-Range Attraction

Masahide Sato

Information Media Center, Kanazawa University,

Kakuma-machi, Kanazawa 920-1192, Japan

(Dated: August 28, 2019)

Abstract

We report on self-assemblies formed from spherical patchy particles interacting by a long-range attraction through a patch region in a two-dimensional system. We performed Monte Carlo simulations to find stable structures in a system with constant number of particles under constant temperature and constant pressure (NPT system), in which particles interact via the Kern–Frenkel potential. For long-range attractive potentials, we describe how these stable structures and their formation depend on the coverage of the patch. Under high pressure, when the coverage is small, triangular lattices are formed as reported in previous papers. From our simulations, we find when the pressure is low short chain-like structures, in which the distance between particles is long, and square clusters, which are not formed with a short-range attractive potential, are formed. When the coverage of the patch region is large, square clusters are formed since the interaction between particles is stronger than that for with small coverage. When the coverage ratio is larger than 0.5, the direction of the patch is perpendicular to the plane in which the particles are placed.

PACS numbers: 61.50.Ah, 81.15.Aa ,81.10.Aj

I. INTRODUCTION

Aggregations and self-assemblies formed with anisotropic particles show characteristic structures and properties which are not displayed by isotropic particles. Hence, anisotropic particles are promising candidates as building blocks of functional materials [1–5]. Recently, many groups designed the anisotropy of colloidal particles by controlling the shape of particles [6–14] and changing the properties of an area of the particle’s surface. When surface properties of a particle are partially changed, the particles are termed patchy.

There have been many studies on how to synthesize patchy particles and what kinds of self-assemblies are produced with them [15–29]. For example, Vissers and co-workers performed Monte Carlo simulations and studied crystals formed from Janus particles [20], namely, spherical particles for which the two halves of the surface have different chemical compositions. By controlling the pressure and the strength of the attractive interaction between the patch areas of the particles, a phase diagram for the structures formed from Janus particles was then developed. The formation of tubes and polymerization of one-patch particles, which are the particles having just one patch region, has also been studied [21, 22]. Structures formed from more complex patchy particles have also been studied [16–19]. Chen and co-workers [16] produced tri-block patchy particles and showed the formation of a colloidal kagome lattice. Chen’s group also studied the self-assemblies formed by multiblock patchy particles [17].

For one-patch particles, the effects of interaction length [26] and coverage of a patch area [23, 27] on structures formed by these particles have already been studied in a three-dimensional system. In these studies, the coverage of the patch area was fixed to one half of the particle’s surface to study the effect of the interaction length [26], and a short interaction length was set when the effect of the coverage of patch area was studied [23]. If we set a longer interaction length and varied the coverage of a patch area, we expect various structures that have not been reported until now to be formed even in a two-dimensional system.

In this paper, we describe how the structures formed by one-patch particles change with increasing the coverage of patch region when the attraction is long-ranged. We expect that the structures formed in two-dimensional systems are simpler than those in three-dimensional systems. Studying such structures is important because two-dimensional regular structures are used as in the colloidal epitaxy method [30] to form regular three-dimensional

structures. In Ref. 27, Iwashita et al. observed the orientational order of patch area and the positional order in thin system for short-range interaction. The authors showed that the orientational order of patch area and the positional order changes intricately with increasing the thickness of the layers. Studying these orders in two-dimensional systems is important to understand how the orders in the two-dimensional system changes with increasing the thickness of the system and how the orders in two-dimensional system are related to those in the three-dimensional system. Therefore, as a first step, we study the two-dimensional structures formed by spherical one-patch particles. The orientational ordering of the patch direction has already been studied assuming that the hexagonal lattice is formed in two-dimensional systems [24, 25]. Studying the orientational order under this assumption is probably reasonable for short-range interactions when the pressure is high. However, if the attractive interaction between patchy particles is long and the pressure is low, it is not obvious whether the hexagonal lattice is formed or not. Thus, to study which structures are produced and how the patchy particles are oriented, we perform isobaric-isothermal (NPT) Monte Carlo simulations using the Kern–Frenkel (KF) potential [31]. In Sec. II, we introduce our model used in NPT simulations and in Sec. III, we present the results of the NPT simulations. In the section, we briefly discuss each result and provide a summary of our results in Sec. IV.

II. MODEL FOR MONTE CARLO SIMULATION

We performed NPT Monte Carlo simulations to study stable structures under given temperatures and pressures. In the simulations, we used the KF potential [31] as an attractive potential between particles. We assume that spherical particles have a one-patch region. For the KF potential [31], the interaction potential of the i th and j th particles is expressed as

$$U_{\text{KF}}(\mathbf{r}_{ij}, \hat{\mathbf{n}}_i, \hat{\mathbf{n}}_j) = U_{\text{rep}}(r_{ij}) + U_{\text{att}}(r_{ij})f(\mathbf{r}_{ij}, \hat{\mathbf{n}}_i, \hat{\mathbf{n}}_j), \quad (1)$$

where \mathbf{r}_i denotes the center of mass for the i th particle, $\mathbf{r}_{ij} = \mathbf{r}_j - \mathbf{r}_i$, $r_{ij} = |\mathbf{r}_{ij}|$, and $\hat{\mathbf{n}}_i = (n_{ix}, n_{iy}, n_{iz})$ represents the direction of the patch region of the i th particle. The first

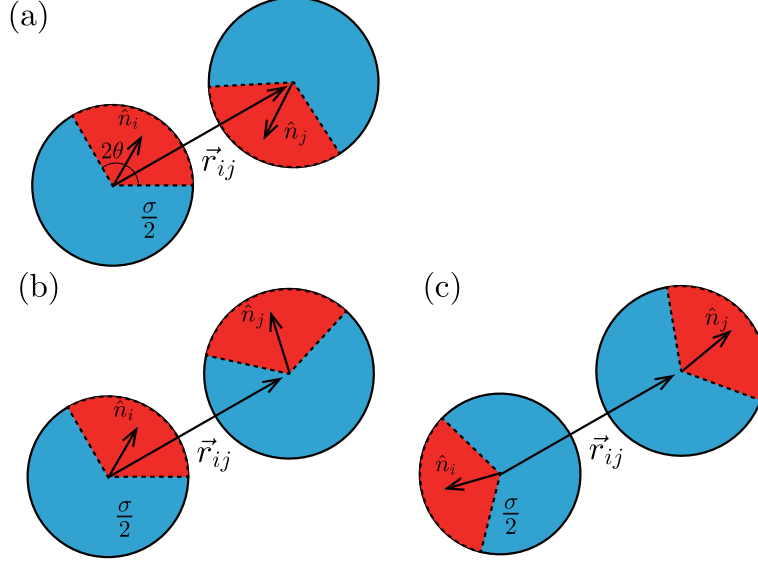


FIG. 1. (color online) Interaction between patchy particles for which the diameter and attractive range are σ and $\Delta/2$, respectively. Patch-facing particles attract each other when their patch areas [red(dark) areas] satisfy the conditions, $\hat{\mathbf{n}}_i \cdot \mathbf{r}_{ij}/|\mathbf{r}_{ij}| > \cos \theta$ and $\hat{\mathbf{n}}_j \cdot \mathbf{r}_{ji}/|\mathbf{r}_{ji}| > \cos \theta$, as in (a), whereas in (b) and (c), their interaction is simply hard-core repulsive.

term $U_{\text{rep}}(r_{ij})$ represents a hard-core repulsive potential, which is given by

$$U_{\text{rep}}(r_{ij}) = \begin{cases} \infty & (r_{ij} \leq \sigma) \\ 0 & (\sigma < r_{ij}) \end{cases}, \quad (2)$$

where σ is the diameter of the patchy particles. The second term in Eq. (1) represents the attractive part of KF potential. $U_{\text{att}}(r_{ij})$ is the square-well potential given by

$$U_{\text{att}}(r_{ij}) = \begin{cases} -\epsilon & (\sigma < r_{ij} \leq \sigma + \Delta) \\ 0 & (\sigma + \Delta < r_{ij}) \end{cases}, \quad (3)$$

where ϵ is a positive parameter representing the well depth and $\Delta/2$ is the attraction range for each particle. $f(\mathbf{r}_{ij}, \hat{\mathbf{n}}_i, \hat{\mathbf{n}}_j)$ describes how the attraction depends on the patch directions of the i th and j th particles and is given by

$$f(\mathbf{r}_{ij}, \hat{\mathbf{n}}_i, \hat{\mathbf{n}}_j) = \begin{cases} 1 & (\hat{\mathbf{n}}_i \cdot \mathbf{r}_{ij}/|\mathbf{r}_{ij}| > \cos \theta \text{ and } \hat{\mathbf{n}}_j \cdot \mathbf{r}_{ji}/|\mathbf{r}_{ji}| > \cos \theta) \\ 0 & \text{otherwise} \end{cases}. \quad (4)$$

where θ is related to the ratio of the patch region to the periphery χ ; specifically, $\chi = (1 - \cos \theta)/2$. Fig. 1 shows the interaction given by the KF potential. Patch-facing parti-

cles attract each other [Fig. 1(a)], otherwise the interaction between particles is repulsive [Figs. 1(b) and (c)].

To study how χ affects two-dimensional structures formed by patch particles, we perform NPT Monte Carlo simulations. In the simulations, we set Δ to $\sigma/2$ and the number of particles N to 256. We consider a square system for which the size is $L \times L$. Initially, we place N patchy particles in the system at random. We move the particles for a long time neglecting the second term of U_{KF} to remove the effect of the initial configuration. Then, we take the attraction term into account and perform translational trials, rotational trials, and trials in which the system size is changed. We tune up the absolute values of translation, rotation, and change in system size to maintain their acceptance ratios above 0.3. For simplicity, instead of checking the Gibbs free energy to assess whether the system has reached an equilibrium state, we monitored the system size and its internal energy. When they seem to be saturated, we consider that the system reaches to an equilibrium state.

III. RESULTS OF MONTE CARLO SIMULATION

We performed Monte Carlo simulations with some values of θ to study how pressure affects the two-dimensional structures for each θ and to identify differences from structures formed by a short-range attraction. First, we show typical structures for some values of θ . Then, we show the phase diagram for some ϵ . Finally, we consider how the structures change with the form of attraction.

A. Structures for $\theta = 15^\circ$

Figure 2 presents snapshots of the structure with $\theta = 15^\circ$. The scaled pressures $P\sigma^3/k_{\text{B}}T$ are 5 for Fig. 2(a) and 40 for Fig. 2(b). In these figures, areas generating an attraction between patchy particles are marked in red; We put small yellow spheres at the centers of particles and draw yellow lines between attracting particles. Dimers of patchy particles are formed in the case of low pressure [Fig. 2(a)]. When the pressure is higher [Fig. 2(b)], the dimers are arranged to form a hexagonal lattice, in which the directions of dimers seem to be at random.

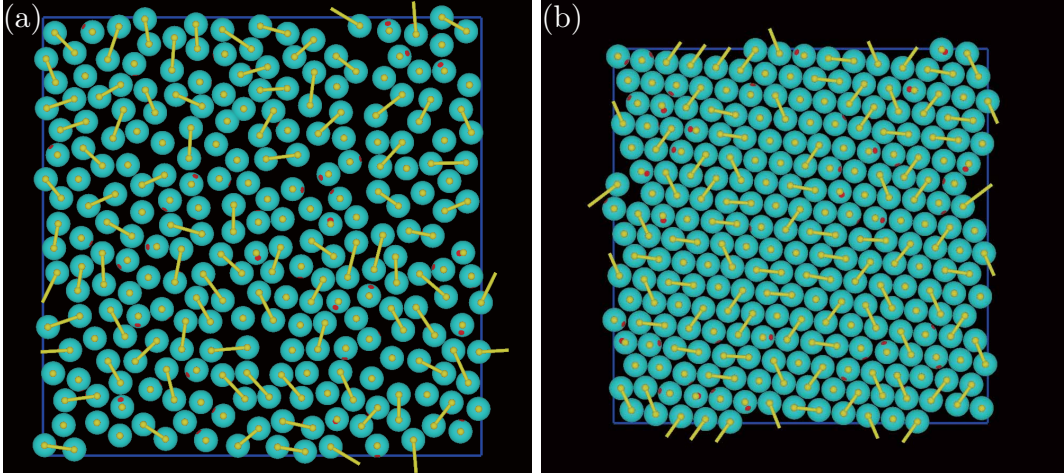


FIG. 2. (color online) Snapshots of two-dimensional structures with $\theta = 15^\circ$ at (a) $P\sigma^3/k_B T = 5.0$ and (b) $P\sigma^3/k_B T = 40$. The red(dark) regions represent the patch areas of attractive interaction between particles under the KF potential; yellow(light) lines mark the connections between particles.

In Fig. 2, clusters larger than dimers are not observed, probably because χ is too small to make large clusters. Figure 3 shows how the number of monomers n_1 and that of dimers n_2 depend on pressure. Because it is reasonable to believe that the system at two different time step in a run are independent if observed at sufficiently long Monte-Carlo step intervals, we averaged the data over 10 points over an interval of 4×10^5 Monte Carlo steps. Taking into account that the number of particles is not so large in our simulations, fluctuations in n_1 and n_2 are inevitable. These numbers appear independent of pressure and roughly the same.

B. Structures for $\theta = 30^\circ$

Figure 4 shows snapshots for $\theta = 30^\circ$. The lattice structure formed under this high pressure is the hexagonal lattice consisting of dimers, which is the same as that formed for $\theta = 15^\circ$ [Fig. 2(b)]. The clusters organized in low pressure [Fig. 4(a)] are different from the dimers shown in Fig. 2(a); zigzag chains of patchy particles have formed under loose attractions as well as compact square tetramers. When $\theta = 30^\circ$ and the interaction length is short enough that the attraction acts between contacting particles, the conditions $\hat{\mathbf{n}}_i \cdot \mathbf{r}_{ij}/|\mathbf{r}_{ij}| > \cos\theta$ and $\hat{\mathbf{n}}_j \cdot \mathbf{r}_{ji}/|\mathbf{r}_{ij}| > \cos\theta$ may not be satisfied in these structures. However, because the attraction range is sufficiently long that distant particles attract each

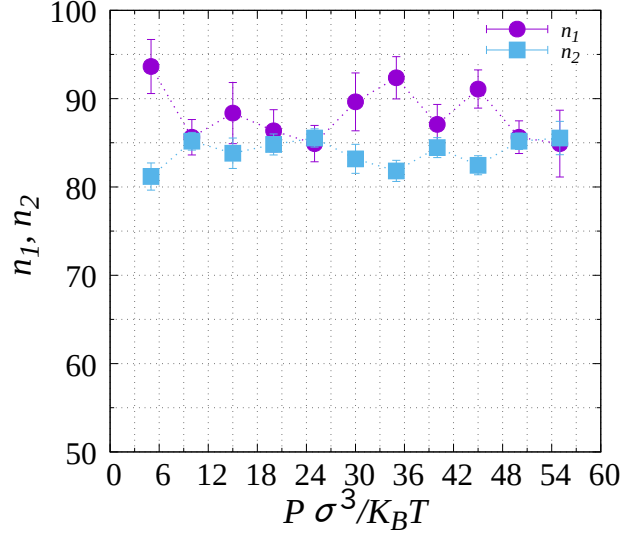


FIG. 3. (color online) Dependence of n_1 and n_2 on pressure for $\theta = 15^\circ$, where n_1 and n_2 represent the numbers of monomers and dimers, respectively. In the later stage of the simulations, data are collected and averaged over 10 points every 4×10^5 MC steps.

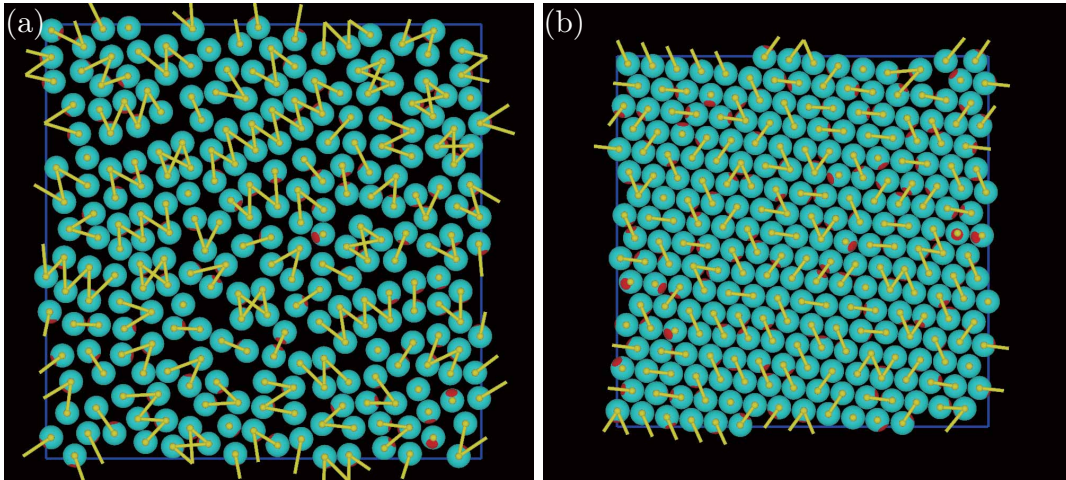


FIG. 4. (color online) Snapshots of two-dimensional structures with $\theta = 30^\circ$ at (a) $P\sigma^3/k_B T = 5.0$ and (b) $P\sigma^3/k_B T = 55$. The significance of the red(dark) regions and yellow(light) lines is the same as given by in Fig. 2.

other, the angle conditions are satisfied and both zigzag chains and compact square tetramers are formed. In particular, patchy particles in the diagonal positions in the compact square tetramers can attract each other because the attraction length is set to be longer than $\sqrt{2}\sigma/2$. Note that in this instance particles in the compact square tetramers do not attract

both neighbors at the same time that angle conditions is only satisfied for one or other of the neighboring particles.

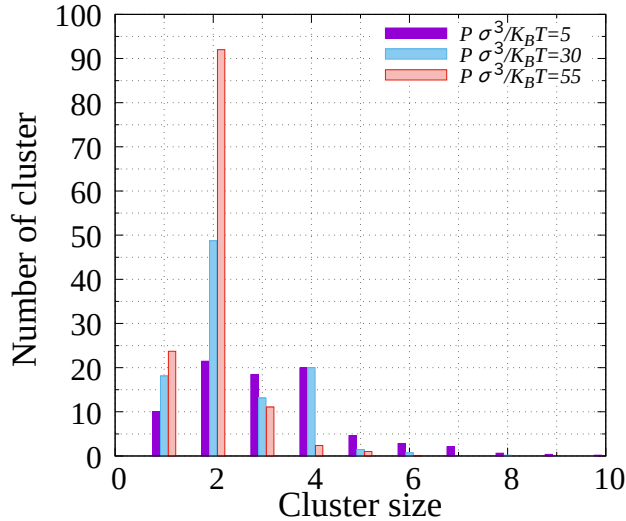


FIG. 5. (color online) Distributions of cluster size at $\theta = 30^\circ$ when $P\sigma^3/k_B T = 5, 30$, and 55 . The data are averaged over 10 points every 4×10^5 MC steps in a late stage. A few numbers of clusters for which the size is larger than 10 are also formed, but the numbers are negligibly small.

Figure 5 presents the distributions of cluster size at $\theta = 30^\circ$ for $P\sigma^3/k_B T = 5, 30$, and 55 . A few clusters consisting of more than 10 particles are formed in our simulations. However, the numbers in those clusters are negligibly small, and hence we only show the data for cluster sizes smaller than 10. Hereafter, we express the number of clusters having i particles as n_i . When $P\sigma^3/k_B T = 5$, the distribution of the cluster size is broad and large clusters are formed. These clusters are mainly zigzag chain-like clusters. n_4 is as large as n_3 because the number of tetramers is included in n_4 . When $P\sigma^3/k_B T = 30$, n_1 and n_2 increase, but with the expectation of n_4 , n_i with $i \geq 3$ decrease. This suggests that loose chain-like structures form with difficulty because, with decreasing the distance between particles under high pressure, the angle conditions $\hat{\mathbf{n}}_i \cdot \mathbf{r}_{ij}/|\mathbf{r}_{ij}| > \cos \theta$ and $\hat{\mathbf{n}}_j \cdot \mathbf{r}_{ji}/|\mathbf{r}_{ij}| > \cos \theta$ are not satisfied. As square tetramers are compact, the effect of increasing pressure on the square tetramers is weak at this pressure and n_4 barely changes. The pressure is so high that the square tetramers are broken when $P\sigma^3/k_B T = 55$. Comparing with the case with $\theta = 15^\circ$, the number of dimers is much larger than that of monomers because the patch area is large enough for dimers to form easily.

C. Structures for $\theta = 40^\circ$

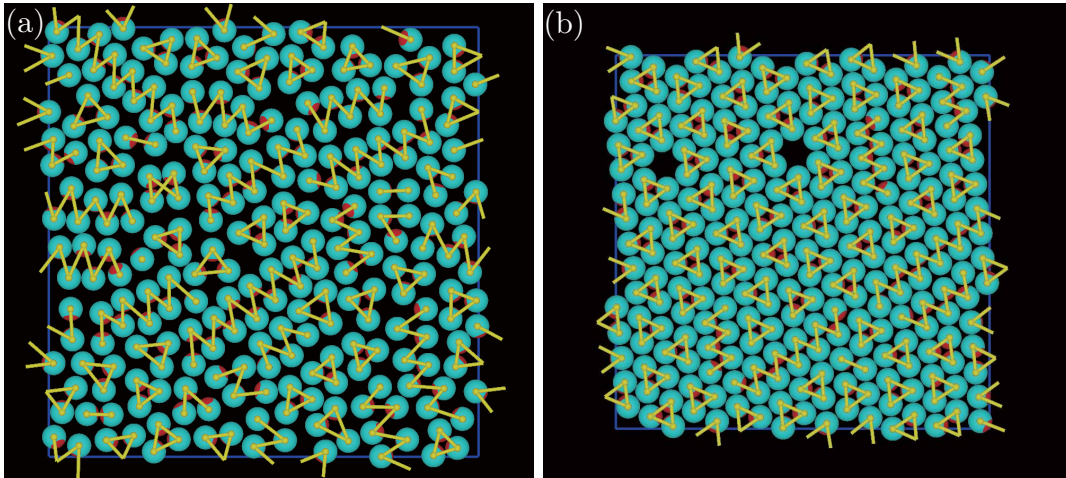


FIG. 6. (color online) Snapshots of two-dimensional structures with $\theta = 40^\circ$ with (a) $P\sigma^3/k_B T = 5$ and (b) $P\sigma^3/k_B T = 45$. The significance of the red(dark) regions and yellow(light) lines is the same as given by in Fig. 2.

When $\theta = 40^\circ$, and triangular trimers are organized under a low pressure in addition to zigzag chain-like clusters [Fig. 6(a)] because χ is large enough for particles in the trimers to attract the other two particles. We observed the zigzag chain-like clusters when $\theta = 30^\circ$ as well, but triangular trimers are formed when $\theta = 40^\circ$. The number of bonds per particle in the trimers is two, which is the same as the bond number per a particle in the tetramers observed in Fig. 4(a). However, since the particle density can be higher when the triangular clusters are formed, the trimers are preferred to tetramers to decrease the system volume. When the pressure is high [Fig. 6(b)], the hexagonal lattice is formed as for $\theta = 15^\circ$ and 30° . However, the attraction of particles is different from these two cases: the hexagonal lattice consists of dimers for $\theta = 15^\circ$ and 30° , but the lattice is formed by triangular trimers for $\theta = 40^\circ$. Figure 7 shows the distributions of cluster size at $\theta = 40^\circ$ for $P\sigma^3/k_B T = 5, 30$, and 45. We can confirm that n_3 is larger than that in the cases of $\theta = 15^\circ$ and 30° , probably as a consequence of the increase in the number of trimers.

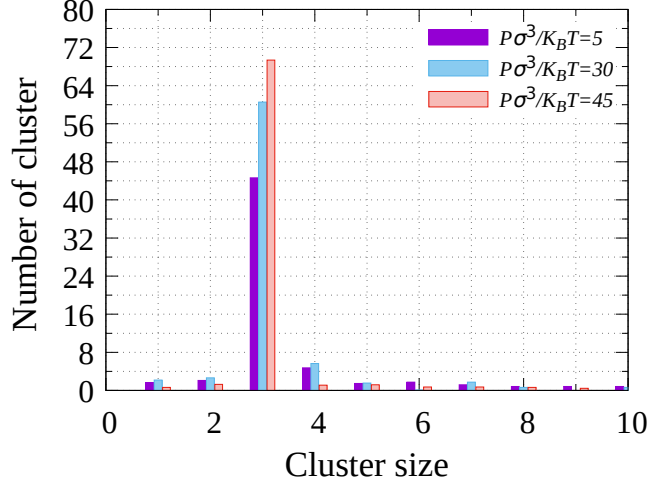


FIG. 7. (color online) Distributions of cluster size at $\theta = 40^\circ$ for $P\sigma^3/k_B T = 5, 30$, and 55 . The data are collected in the late stages and averaged over 10 points every 4×10^5 MC steps. A few numbers of clusters for which the size is larger than 10 are also formed but the numbers are negligibly small.

D. Structures for $\theta = 50^\circ$

Apart from the square tetramers and the loose zigzag chain-like clusters, the other self-assemblies we have showed up to this point were also observed in previous studies [24, 25]. The effect of the long-range attraction on the self-assemblies formed by patchy particles is more obvious when θ is larger than 50° . Figure 8 shows snapshots for $\theta = 50^\circ$. Square tetramers are formed under low pressure [Fig. 8(b)]. Although square tetramers are also shown in Fig. 4(a), the bonding between particles in the clusters is different; the particles in square tetramers do not interact with one of the neighbors when $\theta = 30^\circ$, but the particles interact with all others when $\theta = 50^\circ$ because χ is large [Fig. 8(a)]. When $P\sigma^3/k_B T = 10$ [Fig. 8(b)], a regular array of the square tetramers is formed, which is similar to the formation of a regular array of supraparticles [32, 33].

The structure is close packed with the square as basic unit. When the pressure increases, the square tetramers fragment to increase the particle density, with the square tetramers and triangular trimers coexisting [Fig. 8(c)]. When we carry out simulations with sufficiently high pressure, a hexagonal lattice with triangular trimers forms [Fig. 8(d)].

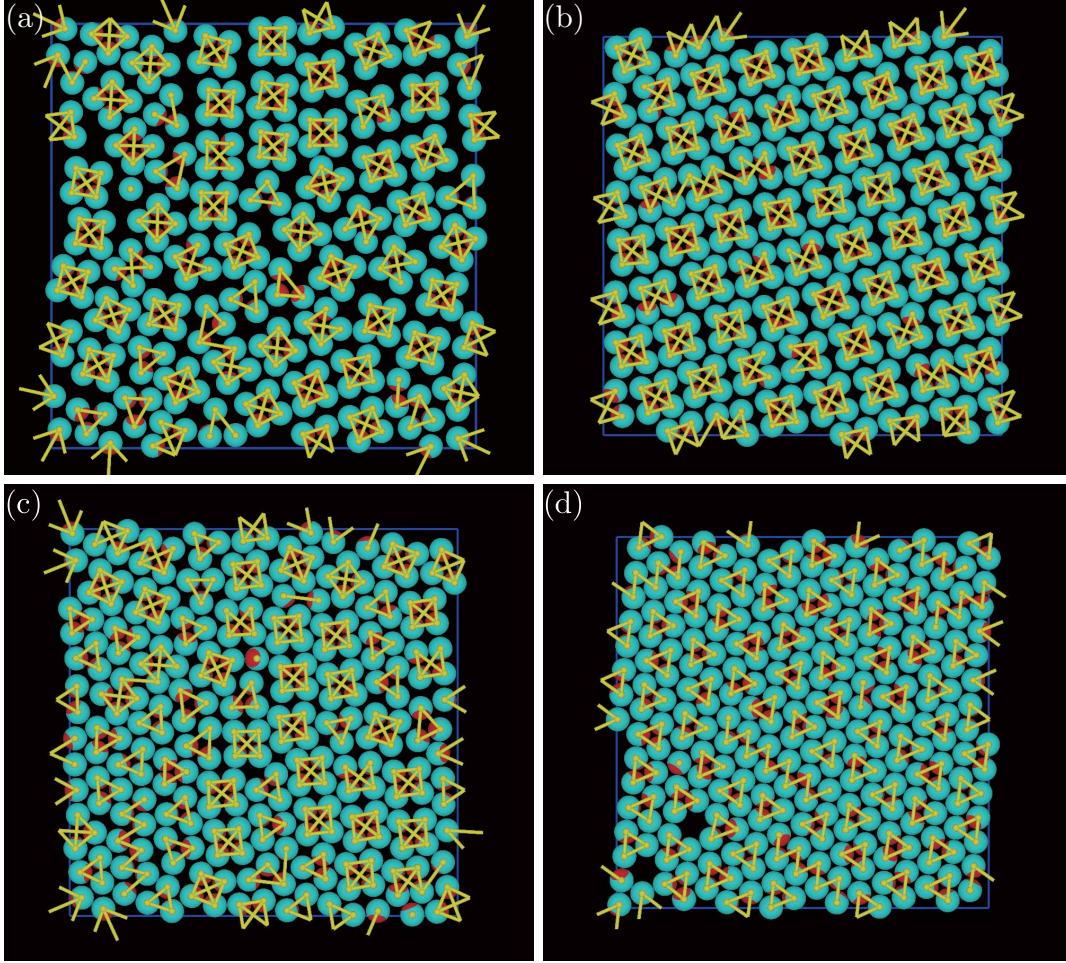


FIG. 8. (color online) Snapshots of two-dimensional structures with $\theta = 50^\circ$ with $P\sigma^3/k_B T$ equal to (a) 5, (b) 10, (c) 25, and (d) 50. The significance of the red(dark) regions and yellow(light) lines is the same as given by in Fig. 2.

We show the distributions of cluster size at $\theta = 50^\circ$ for $P\sigma^3/k_B T = 5, 10, 25,$ and 50 in Fig. 9. When $P\sigma^3/k_B T = 5$, n_4 is larger than n_3 , which means that a small number of triangular tetramers coexist with a large number of square tetramers. When $P\sigma^3/k_B T = 10$, $n_3 = 0$ and n_4 increases, indicating that triangular tetramers are eliminated from the system and almost all clusters are square tetramers. When $P\sigma^3/k_B T = 25$, n_3 increases again, because the triangular trimers form again to increase the density. With the formation of a large peak at n_3 , we believe that most of the clusters become triangular trimers when $P\sigma^3/k_B T = 55$.

When $\theta = 50^\circ$, the structural change induced by increasing the pressure mainly occurs of the transition between triangular trimers and square tetramers. Figure 10 shows the depen-

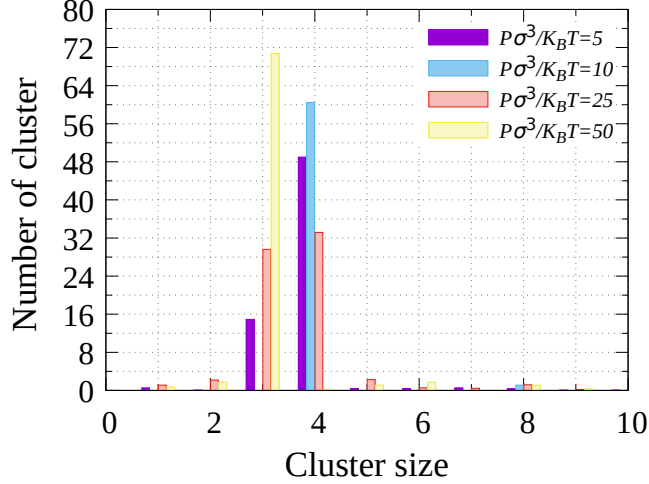


FIG. 9. (color online) Distributions of cluster size at $\theta = 50^\circ$ for $P\sigma^3/k_B T = 5, 10, 25$ and 55 . Data are collected in a late stage and averaged over 10 points every 4×10^5 MC steps. Small numbers of clusters for which the size is larger than 10 are also formed, but the numbers are negligibly small.

dence of n_3 and n_4 on pressure. Unfortunately, the detail dependence is not obvious because of large fluctuations in the data caused by the small number of clusters. Nevertheless, we can find n_3 increases and n_4 decreases with increasing pressure.

E. Structures for $\theta = 80^\circ$

Figure 11 shows snapshots of structures with $\theta = 80^\circ$. In Fig. 11(a), a chain-like structure, in which square tetramers such as B are connected by two bonds such as A has formed because of a large χ value. Hereafter, we refer to this chain-like structure as chain(II). Another chain-like structure, in which triangular trimers or rhomboidal clusters are connected by single bonds, has formed under short-range attraction. This chain-like structure is different from the chain(II) structure because the unit of the chain is a square tetramer in the chain(II). We refer to this chain-like structure as chain(I). When the pressure increases, straight chains of chain(II) are broken and bent at the weakly connected parts consisting of chain(I) [Fig. 11(b)].

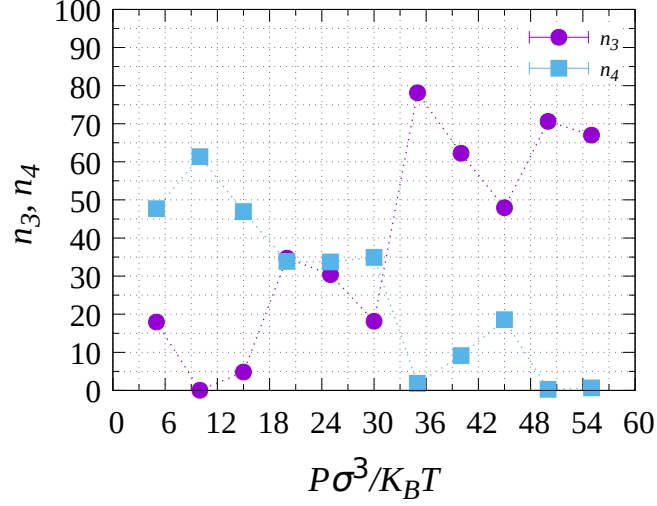


FIG. 10. (color online) Dependence of n_3 and n_4 on pressure at $\theta = 50^\circ$, where n_3 and n_4 represent the numbers of trimers and tetramers, respectively. The data are collected in a late stage and averaged over 10 points every 4×10^5 MC steps.

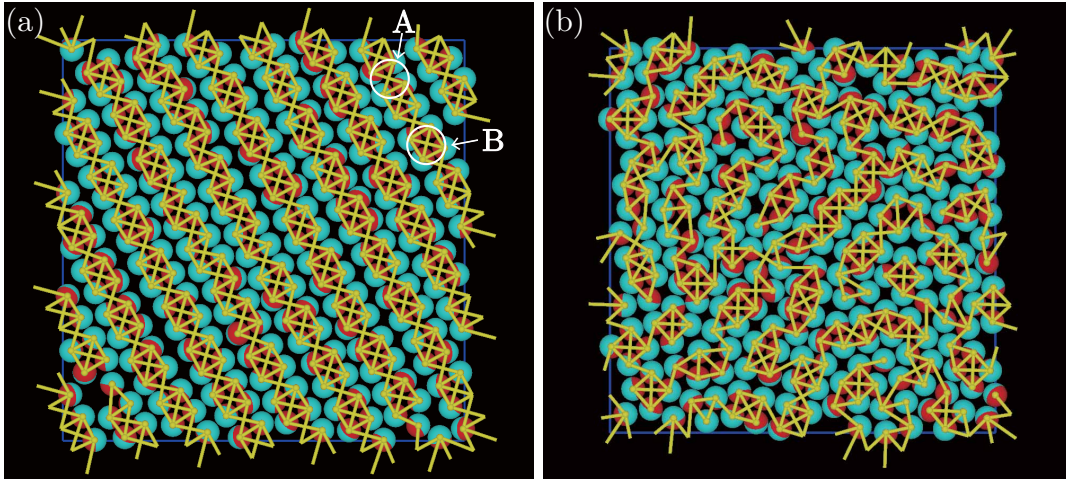


FIG. 11. (color online) Snapshots of two-dimensional structures with $\theta = 80^\circ$ with $P\sigma^3/k_B T$ equal to (a) 5 and (b) 40. The significance of the red(dark) regions and yellow(light) lines is the same as given by in Fig. 2.

F. Structures for $\theta > 90^\circ$

The chain-like clusters shown in Fig. 11 are organized when $\theta \leq 90^\circ$. The structure changes into a square lattice when $\theta > 90^\circ$. Hereafter, we refer to the plane in which

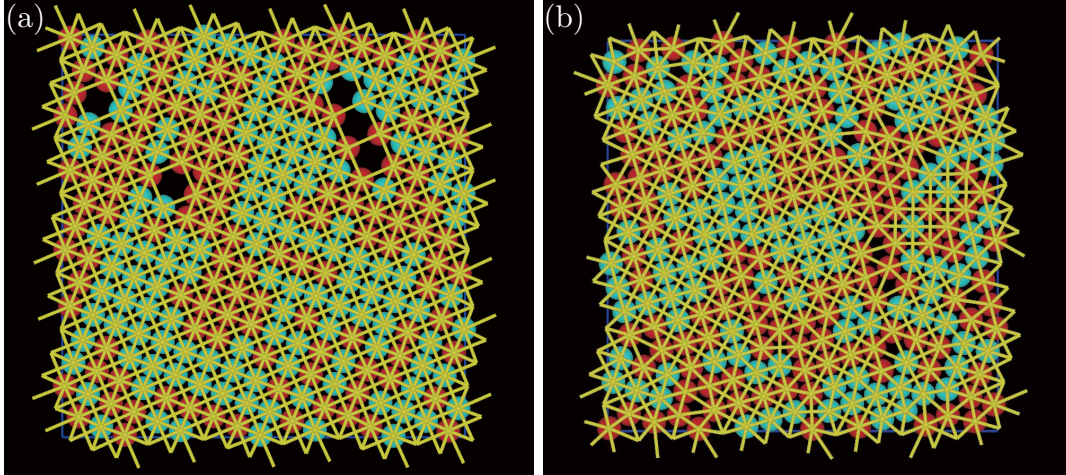


FIG. 12. (color online) Snapshots of two-dimensional structures with $\theta = 95^\circ$ and $P\sigma^3/k_B T$ equal to (a) 15 and (b) 55. The significance of the red(dark) regions and yellow(light) lines is the same as given by in Fig. 2.

the patchy particles are placed as the xy plane and the direction perpendicular to the xy plane as the z -direction. Figure 12 shows snapshots for $\theta = 95^\circ$, in which the direction of the patch region \hat{n} is markedly different from \hat{n} in Figs. 2–11: the component of \hat{n} is predominantly parallel to the xy -plane when $\theta \leq 90^\circ$, but \hat{n} becomes parallel or antiparallel to the z -direction when $\theta > 90^\circ$. The number of connected bonds is no more than five in a square lattice when \hat{n} is in the xy -plane. However, if \hat{n} is in the z -direction, the particles can interact with eight particles at most. Hence, \hat{n} prefers to become perpendicular to the xy -plane to increase the number of interacting particles.

Figure 13 shows the dependence of the average of the absolute value of the component of \hat{n} in the z -direction p_z and that parallel to the xy -plane p_{xy} . They are given by

$$p_z = \left\langle \sum_i |n_{i,z}| \right\rangle, \quad (5)$$

$$p_{xy} = \left\langle \sum_i \sqrt{n_{i,x}^2 + n_{i,y}^2} \right\rangle, \quad (6)$$

where $\langle \dots \rangle$ represents averaging of data in a run with a long interval of MC steps in the late stage. When θ is very small, the attractive interaction between particles barely occurs. Therefore, the direction of the patch area is almost random. The frequency of the formation of dimers increases with increasing θ . Because the directions of the patch areas in dimers should be in the xy -plane, n_z decreases with increasing θ when $\theta < 30^\circ$. When $30^\circ < \theta < 90^\circ$,

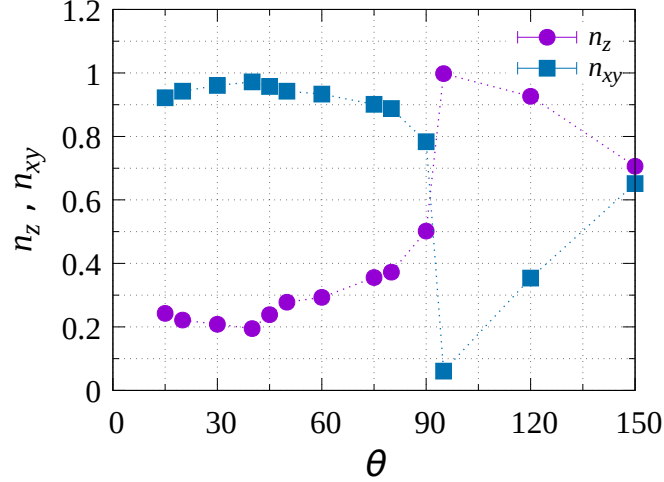


FIG. 13. (color online) Dependence of the amplitude of the component of $\hat{\mathbf{n}}$ in the z -direction n_z and that parallel to the xy -plane n_{xy} on the angle θ , which is related to the coverage of the patch area as $\chi = (1 - \cos \theta)/2$. The dependence is measured for pressure $P\sigma^3/k_B T = 50$ and the data are averaged over 100 points every 4×10^5 MC steps in a run. .

the direction of the patch area fluctuates but maintains an attractive interaction because the patch area is large. Thus, n_z increases gradually with increasing θ . When θ exceeds 90° , n_z increases sharply to increase the number of attracting particles. However, n_z decreases with increasing θ when θ is larger than 90° . The reason is the same as that for decreasing n_{xy} for $30^\circ < \theta < 90^\circ$; that is, $\hat{\mathbf{n}}$ fluctuates but retains the attractive interaction between particles because of the large patch area. The lattice structure probably changes to a hexagonal lattice for short-range attraction. Taking into account that the change in $\hat{\mathbf{n}}$ at $\theta = 90^\circ$ cause the number of attracting particles to increase, we believe that the sharp change is also expected in the hexagonal lattice, which has not been pointed out in previous studies [24, 25].

G. $P\sigma^3/k_B T$ - θ phase diagrams for some $\epsilon/k_B T$

Here, we show $P\sigma^3/k_B T$ - θ phase diagrams for some values. Figure 14 shows the phase diagram for $\epsilon/k_B T = 8$. Here we refer to the square tetramer formed with small θ as tetramer (I) and that formed with large θ as tetramer (II). Hexagonal lattices form when θ is small and the pressure is high. To judge whether hexagonal lattices form, we use a parameter ϕ_6

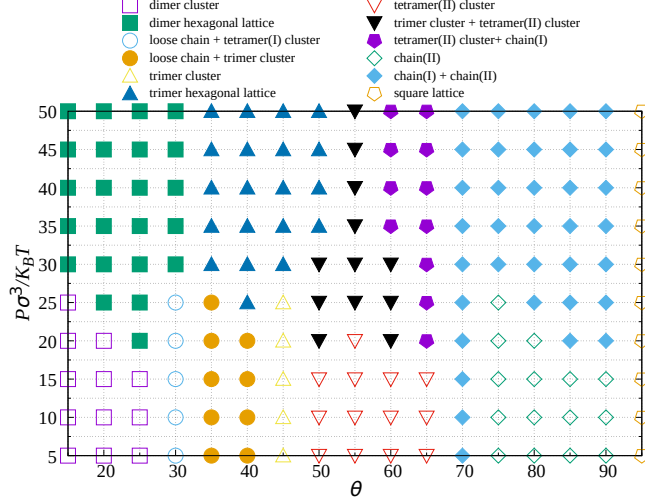


FIG. 14. (color online) $P\sigma^3/k_B T - \theta$ phase diagram for $\epsilon/k_B T = 8$

which shows the local six-fold rotational symmetry. The parameter ϕ_6 is defined as

$$\phi_6 = \frac{1}{N} \sum_i \left| \sum_{r_{ij} < \sigma'} \frac{1}{6} \exp(6i\theta_{ij}) \right|, \quad (7)$$

where θ_{ij} shows the angle between \mathbf{r}_{ij} and x -axis. The summation $\sum_{r_{ij} < \sigma'}$ is performed for the j th particle when $r_{ij} < \sigma'$. We set σ' to 1.2σ because the distance between the nearest neighbors is small when the pressure is high. ϕ_6 should be 1 if the perfect hexagonal lattice forms. However, taking account of thermal fluctuations, we consider that the hexagonal lattice forms when $\phi_6 > 0.7$. When $50^\circ \leq \theta \leq 60^\circ$, the boundary between the phase with tetramer (II) clusters and that with the mixture of tetramer(II) and triangular trimer are determined by the ratio of n_3 to n_4 and snapshots.

We have not shown a snapshot for the phase consisting of tetramer(II) and chain(I). A typical snapshot of this phase is given by Fig. 15. The number of square tetramer(II) decreases with increasing the pressure. When $70^\circ \leq \theta \leq 90^\circ$, the system transfers from the phase of chain(II) to that formed by both chain(I) and chain(II) with increasing the pressure. For simplicity, we determined the phase from snapshots. When θ changes from 90° to 95° , the direction of patch area and the structures formed by particles drastically changes; the direction of patch area is parallel or antiparallel to the z -axis and particles form a square lattice.

Figure 16 shows how the phase diagram changes with decreasing $\epsilon/k_B T$. When $\epsilon/k_B T = 6$

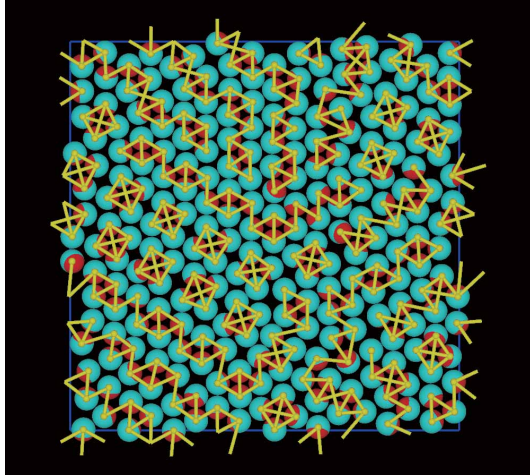


FIG. 15. (color online) Snapshots of two-dimensional structures with $\theta = 65^\circ$ and $P\sigma^3/k_B T = 30$. The significance of the red(dark) regions and yellow(light) lines is the same as given by in Fig. 2.

[Fig. 16(a)], square tetramers and chain(II) form when the pressure is low and θ is large, but the areas in which those structures form are slightly smaller than those in Fig. 14. When $\epsilon/k_B T = 4$ [Fig. 16(b)], the structures which are caused by the square tetramers disappear; the clusters of the square tetramer, the chain(II), and the mixture of chain (I) and chain (II) do not form. When $\theta = 95^\circ$, the region with a hexagonal lattice appears under high pressure although the patch direction in the region is parallel or antiparallel to the z -axis. When $\epsilon/k_B T = 4$ [Fig. 16(c)], triangular trimers and the hexagonal lattice formed by them do not form. Dimers and hexagonal lattice formed by dimers appear instead. In the regions where these structures form, triangular trimers and short zigzag chain appear with increasing θ , but the their numbers are very small.

H. Effect of the form of U_{att} on structures

In our simulations, a main difference from previous studies [24, 25] is the formation of square tetramers. Since Δ is set to $\sigma/2$, the particles in the diagonal positions can attract each other in the square cluster whose side length is σ . We think that the square tetramers do not form when $\Delta \leq (\sqrt{2}-1)\sigma$ because the attraction between the particles in the diagonal positions in the square tetramers vanishes.

To confirm the prediction, we set Δ to $0.3\sigma < (\sqrt{2}-1)\sigma$ and performed simulations. Figures 17(a) and (b) show snapshots for $\theta = 60^\circ$ and $\theta = 80^\circ$. Square tetramers observed

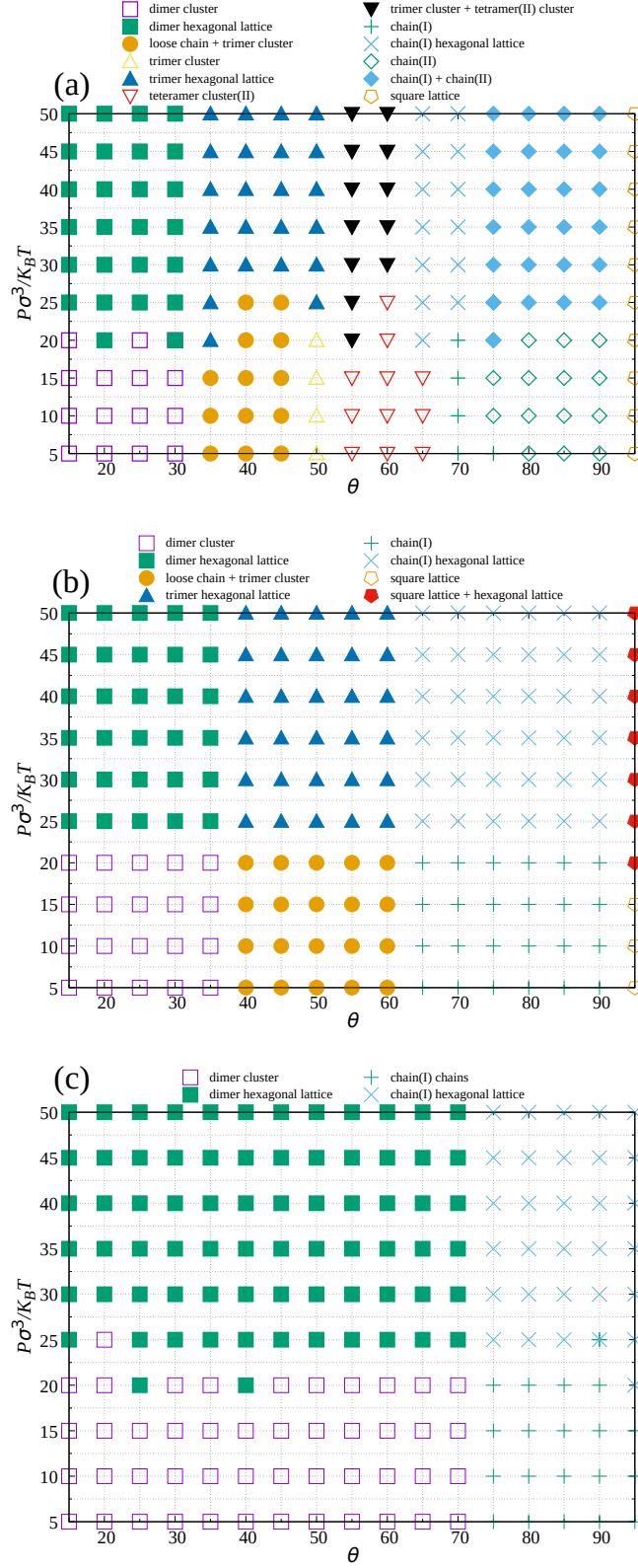


FIG. 16. (color online) $P\sigma^3/k_B T - \theta$ phase diagrams for $\epsilon/k_B T =$ (a) 6, (b) 4, and (c) 1.

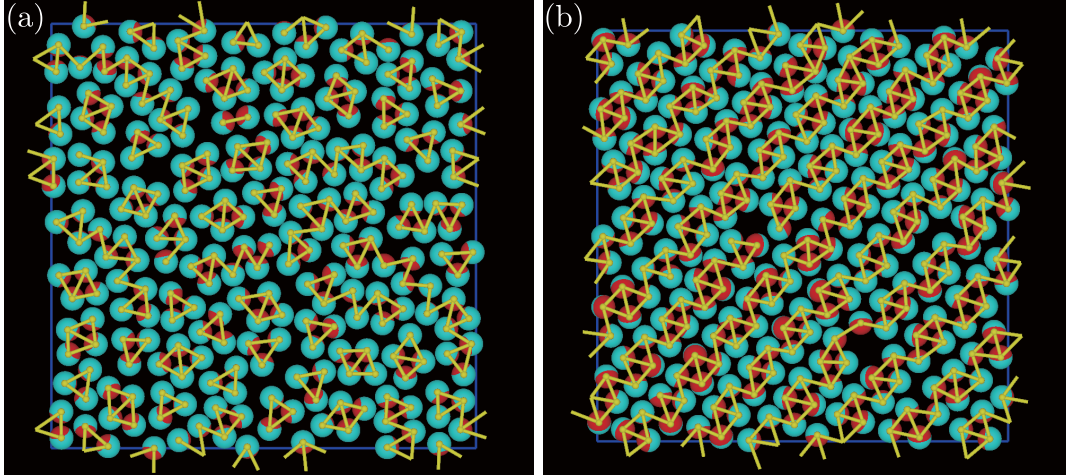


FIG. 17. (color online) Snapshots of two-dimensional structures for $\theta =$ (a) 60° and (b) 80° . $P\sigma^3/k_B T$ equal to 5 and Δ is set to 0.3. The significance of the red(dark) regions and yellow(light) lines is the same as given by in Fig. 2.

in Fig. 8 do not form in Fig. 17(a), and triangular trimers and rhomboidal clusters form instead [Fig. 17(a)]. The form of chains also changes from chain (II) to chain (I) when $\theta = 80^\circ$ [Fig. 17(b)]. The structure for $\theta > 90^\circ$ also changes. The direction of patch area for

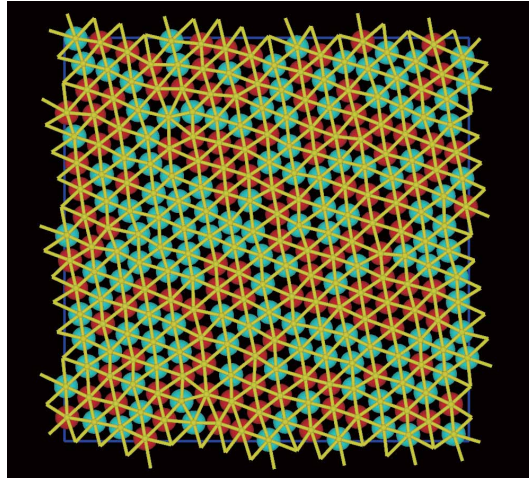


FIG. 18. (color online) A snapshot of two-dimensional structure with $\theta = 95^\circ$, $\Delta = 0.3\sigma < (\sqrt{2} - 1)\sigma$, and $P\sigma^3/k_B T = 5$. The significance of the red(dark) regions and yellow(light) lines is the same as given by in Fig. 2.

each particle is perpendicular to the plane where the particles are located, but the square lattice observed in Fig. 12 changes to the hexagonal lattice as shown in Fig. 18. These

results agree with our prediction.

We also performed simulations using the Lennard-Jones (LJ) potential as $U_{\text{att}}(r)$. We considered the hard-core repulsive potential when $r_{ij} < 2^{1/6}\sigma$. $U_{\text{att}}(r_{ij})$ is given by

$$U_{\text{att}}(r_{ij}) = 4\epsilon \left\{ \left(\frac{\sigma}{r} \right)^{12} - \left(\frac{\sigma}{r} \right)^6 \right\} \quad (2^{1/6}\sigma < r_{ij}). \quad (8)$$

We set $\epsilon/k_{\text{B}}T = 8$ in the simulations for the minimum of the attractive potential to be $-\epsilon$. Figures 19(a) and (b) show snapshots for $\theta = 55^\circ$ and 85° , respectively. When $U_{\text{att}}(r)$ is

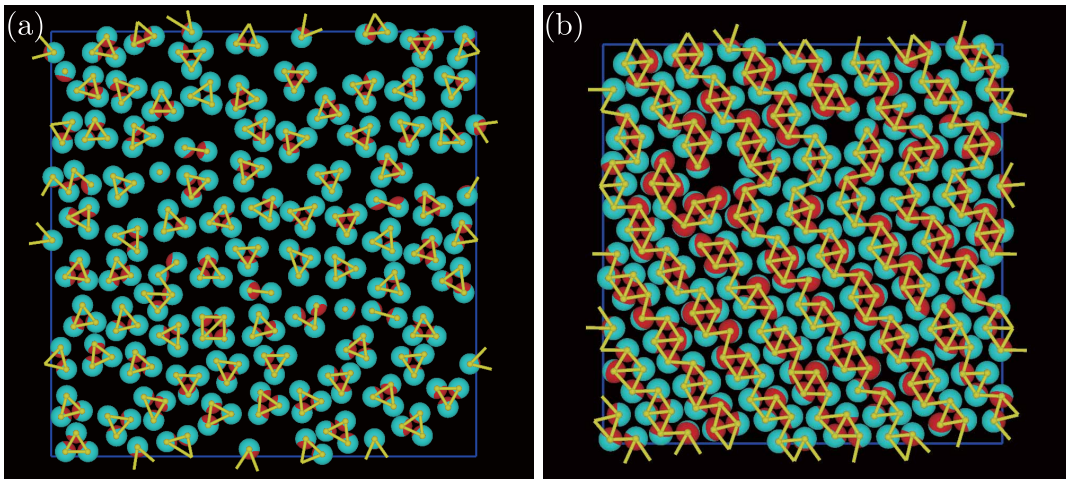


FIG. 19. (color online) Snapshots of two-dimensional structures for the LJ attractive potential. θ and $P\sigma^3/k_{\text{B}}T$ are (a) 55° and 5 and (b) 85° and 10, respectively. The significance of the red(dark) regions is the as given by in Fig. 2. yellow(light) lines are drawn when the distance between the centers of particles is smaller than $2^{1/6}\sigma$.

the square wall potential with $\Delta = \sigma/2$, the square tetramers and chain (II) form for these θ . However, when the attractive potential is the LJ potential, triangular trimers and single chains form instead to increase the number of the nearest neighbors.

Figure 20 shows a snapshot for $\theta = 95^\circ$. Although large voids remain even with the high pressure, the hexagonal lattice forms for the LJ potential as well as for the square wall potential with $\Delta < \sigma/2$ because the number of the nearest neighbors is the largest in the hexagonal lattice.

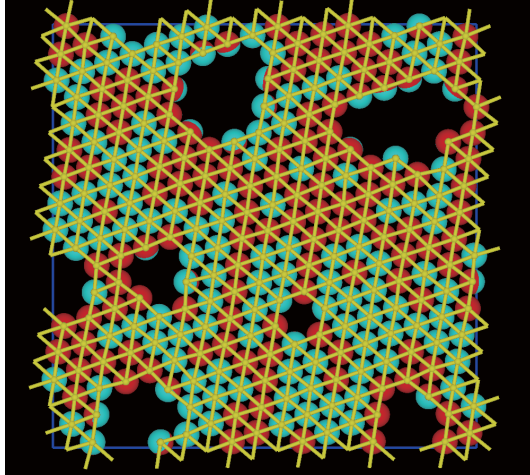


FIG. 20. (color online) Snapshots of two-dimensional structures for the LJ attractive potential. $\theta = 95^\circ$ and $P\sigma^3/k_B T = 30$. The significance of the red(dark) regions yellow(light) lines is the same as given by Fig. 19

IV. SUMMARY

We performed both Monte Carlo simulations and Brownian dynamics simulations to study self-assemblies formed by one-patch particles. Using the KF potential in Monte Carlo simulations, we studied how the self-assemblies with long-range attractive interactions differ from those with short-range attractive interactions. The clusters formed in low pressure changed from dimers to triangle trimers with increasing χ . Square tetramers, chains formed by square tetramers, and islands with a square lattice are also formed with further increase in χ .

Although the system size of our simulations is not so large, we obtained new results. The main difference between our results and previous results from a short-range attractive interactions is the formation of loose zigzag chain and square tetramers. The loose zigzag chain is observed when χ is small. In our simulations, two types of square tetramers are formed. When χ is small, the particles in the square tetramers interact with one of neighbors and the particle in the diagonal position but do not interact with the other neighbor. In the other, when χ is large, the particles in the square tetramers can interact with all other particles. These self-assemblies form under low pressure.

The other main result is that the patch direction \hat{n} changes at $\theta = 90^\circ$ when $\epsilon/k_B T \geq 6$. \hat{n} is in the plane where the particles are located when $\theta \leq 90^\circ$, but changes sharply to

lie perpendicular to the plane when θ exceeds 90° . The change in $\hat{\mathbf{n}}$ is not because of a long-range attraction. As the direction of the patch region changes to increase the number of neighbors, the same change in $\hat{\mathbf{n}}$ should also occur for short-range attraction. The point has not been mentioned in the literature [24, 25]

In our simulations, the formation of new types of self-assemblies arise from the square wall like long-range attraction. It may be difficult to realize experimentally such long-range attractions, but we suggest that coating particles with DNA strands is one possible method to create the potential. Currently, designing DNA freely and controlling the interaction between particles to produce a structure as desired is becoming possible [34–40]. We remain hopeful that patchy particles with long-range attractive potentials are realized through this technique.

ACKNOWLEDGMENTS

This work was supported by JSPS KAKENHI Grants, Nos. JP16K05470, JP18K04960, and JP18H03839, and the Grant for Joint Research Program of the Institute of Low Temperature Science, Hokkaido University, Grant number 19G020.

-
- [1] Z. Zhang and S. C. Glotzer, *Nano Lett.* **4**, 1407 (2004)
 - [2] M. Maldovan and E. L. Thomas, *Nat. Mater.* **3**, 593 (2004).
 - [3] K.-H. Roh, D. C. Martin, and J. Lahann, *Nat. Mater.* **4**, 759 (2005).
 - [4] Y. Wang, Y. Wang, D. R. Breed, V. N. Manoharan, L. Feng, A. D. Hollingsworth, M. Weck, and D. J. Pine, *Nature (London)* textbf491, 51 (2012).
 - [5] X. Mao, Q. Chan, and S. Granick, *Nat. Mater.* **12**, 217 (2013).
 - [6] S. C. Glotzer, and M. J. Solomon, *Nat. Mater.* **6**, 557 (2007).
 - [7] S. Sacanna, W. T. M. Irvine, P. M. Chaikin, and D. J. Pine, *Nature (London)* **464**, 575 (2010).
 - [8] M. R. Jones, R. J. Macfarlane, B. Lee, J. Zhang, K. L. Young, A. J. Senesi, and C. A. Mirkin, *Nat. Mater.* **9**, 913 (2010).
 - [9] D. J. Kraft, J. Hihorst, M. A. P. Heinen, M. J. Hoogenraad, B. Luigjes, and W. K. Kegal, *J. Phys. Chem. B* **115**, 7175 (2011).

- [10] D. J. Kraft, R. Ni, F. Smalenburg, M. Hermes, K. Yoon, D. A. Weitz, A. v. Blaaderen, J. Groeneveld, M. Dijkstra, and W. K. Kegel, *Proc. Natl. Acad. Sci.* **109**, 10787 (2012).
- [11] G. Avvisati, T. Vissers, and M. Dijkstra, *J. Chem. Phys.* **142**, 084905 (2015).
- [12] J. J. Geuchies, C. van. Overbeek, W. H. Evers, B. Goris, A. de. Becker, A. P. Gantapara, F. T. Rabouw, J. Hilhorst, J. L. Peters, O. Konovalov, A. V. Petukhov, M. Dijkstra, L. D. A. Siebbeles, S. van. Aert, S. Bals, and D. Vanmaekelbergh *Nat. Mater.* **15**, 1 (2016).
- [13] J. R. Wolters, J. E. Verweij, G. Avvisati, M. Dijkstra, and W. K. Kegel, *Langmuir* **33**, 3270 (2017).
- [14] c. Kang and A. Honciuc, *ACS Nano* **12**, 3741 (2018).
- [15] W. L. Miller and A. Cacciuto, *Phys. Rev. E* **80**, 021404 (2009).
- [16] Q. Chen, S. C. Bae, and, S. Granick, *Nature* **469**, 381 (2011).
- [17] Q. Chen, J. K. Whitmer, S. Jiang, S. C. Bae, E. Luijten, and S. Granick, *Science* **331**, 199 (2011).
- [18] Q. Chen, J. Yan, J. Zhang, S. C. Bae, and S. Granick, *Langmuir* **28**, 13555 (2012).
- [19] F. Romano, E. Sanz, P. Tartaglia, and F. Sciortino, *J. Phys.: Condens. Matter* **24**, 064113 (2012).
- [20] T. Vissers, Z. Preisler, F. Smalenburg, M. Dijkstra, and F. Sciortino, *J. Chem. Phys.* **138**, 164505 (2013).
- [21] Z. Preisler, T. Vissers, F. Smalenburg, G. Munaò, and F. Sciortino, *J. Phys. Chem. B* **117**, 9540 (2013).
- [22] T. Vissers, f. Smalenburg, G. Munaò, Z. Preisler, and F. Sciortino, *J. Chem. Phys.* **140**, 144902 (2014).
- [23] Z. Preisler, T. Vissers, G. Munaò, f. Smalenburg, and F. Sciortino, *Soft Matter* **10**, 5121 (2014).
- [24] H. Shin and K. S. Schweizer, *Soft Matter* **10**, 262 (2014).
- [25] Y. Iwashita and Y. Kimura, *Soft Matter* **10**, 7170 (2014).
- [26] Z. Preisler, T. Vissers, F. Smalenburg, and F. Sciortino, *J. Chem. Phys.* **145**, 064513 (2016).
- [27] Y. Iwashita and Y. Kimura, *Sci. Rep.* **6**, 27599 (2016).
- [28] Z. Gong, T. Hueckel, G.-R. Yi, and S. Sacanna, *Nature* **550**, 234 (2017).
- [29] N. Patra and A. V. Tkachenko, *Phys. Rev. E* **96**, 022601 (2017).
- [30] A. van Blaaderen, R. Ruel, and P. Wiltzius, *Nature (London)* **385**, 321 (1997).

- [31] N. Kern and D. Frenkel, *J. Chem. Phys.* **118**, 9882 (2003).
- [32] Y. Xia, T. D. Nguyen, M. Yang, B. Lee, A. Santos, P. Podsiadlo, Z. Tang, S. C. Glotzer, and N. A. Kotov, *Nat. Nanotechnol.* **6**, 580 (2011).
- [33] T. D. Nguyen, B. A. Schultz, N. A. Kotov, and S. C. Glotzer, *Proc. Natl. Acad. Sci.* **112**, E3161 (2015).
- [34] D. Nykypanchuk, M. M. Maye, D. van der Lelie, and O. Gang, *Nature* **451**, 549 (2008).
- [35] S. Y. Park, A. K. R. Lytton-Jean, B. Lee, S. Weigand, G. C. Schatz, and C. A. Mirkin, *Nature* **451**, 553 (2008).
- [36] R. J. Macfarlane, B. Lee, H. D. Hill, A. J. Senesi, S. Seifert, and C. A. Mirkin, *Proc. Natl. Acad. Sci. U.S.A.* **106**, 10493 (2009).
- [37] R. J. Macfarlane, B. Lee, M. R. Jones, N. Harris, G. C. Schatz, and C. A. Mirkin, *Science* **334**, 204 (2011).
- [38] C. Zhang, R. J. Macfarlane, K. L. Young, C. H. J. Choi, L. Hao, E. Auyeung, G. Liu, X. Zhou, and C. A. Mirkin, *Nat. Mater.* **12**, 741 (2013).
- [39] T. Isogai, A. Piednoir, E. Akada, Y. Akahosi, R. Tero, S. Harada, T. Ujihara, and M. Tagawa, *J. Cryst. Growth* **401**, 494 (2014).
- [40] T. Isogai, E. Akada, S. Nakada, N. Yoshida, R. Tero, S. Harada, T. Ujihara, and M. Tagawa, *Jpn. J. Appl. Phys.* **55**, 03DF11 (2016).